ARTICLE

Chinese Journal of Structural Chemistry

K_2HPO_4-mediated Photocatalytic H_2 Production over NiCoP/RP Heterojunction

Junfeng Huang[1], Chenyang Li[1], Xiaoyun Hu[2], Jun Fan[1], Binran Zhao[1]* and Enzhou Liu[1]*

[1]*School of Chemical Engineering/Xi'an Key Laboratory of Special Energy Materials, Northwest University, Xi' an 710069, China*
[2]*School of Physics, Northwest University, Xi'an 710069, China*

ABSTRACT In this work, bimetallic NiCoP nanoparticles (NPs) were firstly prepared by a solvothermal method using red phosphorus (RP) as P source, and it was combined with RP nanosheets *via* a physical grinding process. Investigation indicates that NiCoP has better charge transfer ability and faster H_2 releasing kinetics than the corresponding single metal phosphides alone. 6 *wt*% NiCoP/RP exhibits an excellent H_2 evolution activity in 20 *vol.*% triethanol-amine/water solution under a 300W Xe-lamp irradiation, and the corresponding H_2 production rate is 1535.6 μmol·g^{-1}·h^{-1}, which is 7.4, 3.2 and 2.6 times higher than those of pure RP, 6 *wt*% Co_2P/RP and 6 *wt*% Ni_2P/RP, respectively. In addition, we demonstrate that K_2HPO_4 can further enhance the H_2 evolution kinetics by inducing a new H^+ reduction path, when appropriate K_2HPO_4 is introduced into the reaction solution. The H_2 production rate of 6 *wt*% NiCoP/RP is boosted from 1535.6 to 2793.9 μmol·g^{-1}·h^{-1} due to the easier combination between H^+ and electrons with the assistance of HPO_4^{2-}. It is 13.4 times higher than that of pure RP. This work demonstrates that bimetallic phosphides with suitable electrolytes can greatly enhance the photocatalytic H_2 evolution efficiency.

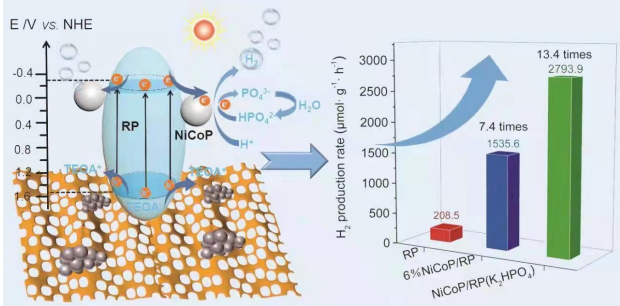

Keywords: photocatalysis, hydrogen, red phosphorus, bimetallic cocatalyst, K_2HPO_4

n INTRODUNTION

As a sustainable and renewable energy carrier, H_2 is one of the candidates to replace traditional fossil energy to achieve carbon-neutrality because of its high calorific value and environmental friendly features.[1-3] About 50 years ago, Fujishima et al. discovered the photocatalytic water splitting over TiO_2 anode and Pt cathode under ultraviolet light.[4] Hereafter, photocatalysis has been considered as a promising strategy to solve energy and environment-related issues based on the redox reaction induced by the photo-generated electrons and holes,[5] such as CO_2 reduction,[6] water splitting,[7] contaminant purification,[8] N_2 fixation,[9] bacterial inactivation,[10] etc. However, photocatalysts with wide band gap can only be excited by UV light, leading to a lower energy utilization efficiency,[11] such as TiO_2,[12] ZnO,[13] and $SrTiO_3$.[14] Besides, g-C_3N_4,[15] CdS,[16] ZnSe[17] and so on with narrow band gap can only harvest parts of visible light, some of which also suffer from poor stability and toxicity.[18] At present, it is urgent to develop photocatalysts with good stability and nontoxicity, especially excellent visible light capturing ability.

In 2012, Yu et al. first discovered that red phosphorus (RP) can achieve photocatalytic H_2 evolution from water based on the experimental and theoretical investigations.[19] What's more, RP can absorb almost all of the visible light for its suitable band gap (~1.8 eV), and can also achieve overall water splitting for its appropriate conduction band (CB) and valence band (VB) positions.[20] These trigger the wide attention to develop RP-based photocatalysis systems from the researchers. Hereafter, fibrous RP was deposited on the surface of SiO_2 fibers *via* a chemical vapor deposition (CVD) process by Hu et al. It is found that fibrous RP with small size demonstrated best H_2 production activity among the element photocatalysts, including silicon (Si), boron (B), carbon (C), sulfur (S) and selenium (Se).[21]

Although RP has been widely used in the photocatalytic H_2 evolution reaction (HER) for its ideal light absorption and suitable band structures, the practical application of it is severely restricted by its low surface area and fast charge recombination.[22,23] Many strategies have been employed to address these inherent drawbacks, such as reducing size,[24] constructing heterojunctions,[25] and loading co-catalyst.[26] Among them, loading noble metal co-catalysts like Pt,[27] Au[28] and Ag[29] are a better strategy, but it is impossible for a large-scale application due to their scarcity.[30] Therefore, it is highly urgent to explore an inexpensive non-precious metal cocatalyst with desired activity.[31]

Transition metal phosphides (TMPs), such as Ni_2P,[32] $Ni_{12}P_5$,[33] Co_2P,[34] and Cu_3P,[35] have been proved as "Pt like" co-catalysts in HER.[36,37] They can not only accelerate the separation and migration of charge carries, but also restrict the electron delocalization in the metal for protons trapping effect of P atom, thus effectively improving their HER activity.[38-40] Zhang et al. synthesized Ni_2P electrocatalysts in an oil phase *via* a hot-bubbling method, which achieved a notable HER activity by decreasing the H_2 releasing over-potential about 35 mV.[41] Zhang et al. demonstrated that CoP_3/Ni_2P heterostructure can provide more active centers based on the DFT calculation. It exhibited an excellent HER and OER activity in a wide pH range.[42] Nevertheless, the preparation of TMPs usually requires toxic phosphorus sources, inert gas protection and high temperature, which is a headache for the application of TMPs.

In this work, a series of NiCoP/RP heterojunctions were prepared

Chin. J. Struct. Chem. **2022**, 41, 2206062-2206068
DOI: 10.14102/j.cnki.0254-5861.2021-0055

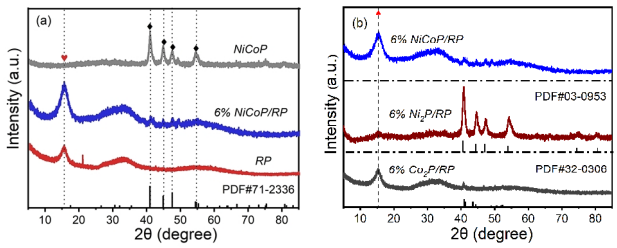

Figure 1. XRD patterns of samples.

by a physical grinding process. The H_2 production rate of 6 *wt*% NiCoP/RP is 1535.6 μmol·g^{-1}·h^{-1} in 20 *vol*.% TEOA aqueous solution, which can be further boosted to 2793.9 μmol·g^{-1}·h^{-1} after adding appropriate K_2HPO_4. Besides, K_2HPO_4-assisted H_2 production mechanism over NiCoP/RP heterojunction is investigated based on the structural characterization and photoelectric analysis.

n RESULTS AND DISCUSSION

Structural Characterization. Figure S2 shows the XRD patterns of the samples. The diffraction intensity of NiCoP increases obviously with the increase of the amount of Ni^{2+}, indicating Ni^{2+} can promote the formation of bimetallic phosphides. The peaks at 40.8°, 44.7°, 47.4° and 54.5° correspond to (111), (201), (210) and (002) planes of hexagonal phase NiCoP (PDF#71-2336), respectively.[43] It's worth noting that the signal of $Ni_{12}P_5$ at 48.9° appears (PDF#74-1381) in $Ni_{1.25}Co_{0.75}P$ and $Ni_{1.5}Co_{0.5}P$.[44] Thereby, it is benefit to form $Ni_{12}P_5$ when the amount of Ni^{2+} is excessive. In this work, NiCoP with good crystallinity was selected as the co-catalyst of RP for H_2 production. The signals of both RP and NiCoP are observed in the XRD pattern of 6% NiCoP/RP in Figure 1a, indicating they are successfully combined together after the physical grinding process. For comparison, 6% Ni_2P/RP and 6% Co_2P/RP were also prepared. As shown in Figure 1b, the peaks of Ni_2P/RP at 40.8°, 44.6°, 47.3°, 54.2°, 72.7° and 74.3° correspond to (111), (201), (210), (300), (311) and (400) planes of Ni_2P (PDF#03-0953), respectively.[45] The peaks of Co_2P/RP at 40.7°, 43.29° and 52.46° belong to (121), (211) and (002) planes of orthorhombic phase Co_2P (PDF#32-0306).[46]

The morphology of the samples was firstly observed by scanning electron microscope (SEM). The surface of RP is smooth and porous in Figure S3(a-b).[47] However, the surface of the sample becomes rough after introducing NiCoP in Figure S3(c-d). It is clear that some nanoparticles are located on the surface of RP. At the same time, Ni, Co and P can be detected by elemental mapping. The atomic ratio of Ni and Co is about 1:1, which is consistent with the stoichiometric ratio of NiCoP. Subsequently, the microstructures of the samples were further observed by TEM. Clearly, NiCoP NPs with a particle size of 30-50 nm are loaded on the two-dimensional honeycomb-like RP surface in Figure 2. The lattice space of 0.225 nm results from the (111) crystal plane of NiCoP NPs, implying NiCoP is successfully introduced into the surface of RP nanosheets.[48]

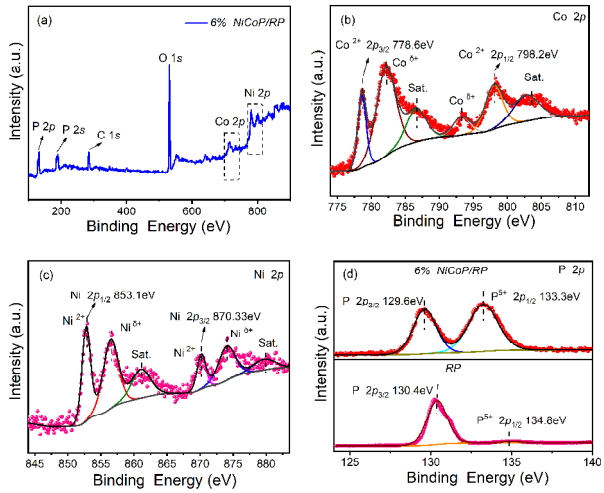

Figure 3. XPS survey spectra of (a) 6% NiCoP/RP. The high-resolution XPS spectra of (b-d) Co 2*p*, Ni 2*p* and P 2*p*.

The N_2 adsorption-desorption isotherm plots of the samples is in Figure S4. The specific surface area (S_{BET}) of 6% NiCoP/RP is 62.66 m^2·g^{-1}, which is higher than that of RP (32. 80 m^2·g^{-1}) after physical grinding process, during which the relative compressive force perpendicular to the surface of RP increases the shear force, leading to an increased S_{BET}.[49] The higher S_{BET} can not only provide more active sites for the H_2 production, but also promote the adsorption and migration of target molecules, which is conducive to the photocatalytic reaction.[50,51]

In order to investigate the surface element composition and state of the composite, 6% NiCoP/RP was characterized by XPS. As shown in Figure 3a, besides O 1*s*, C 1*s* and P 2*p*, the signals of Ni 2*p* and Co 2*p* are also observed. The peaks at 778.6 eV ($2p_{3/2}$) and 798.2 eV ($2p_{1/2}$) in Figure 3b correspond to the peaks

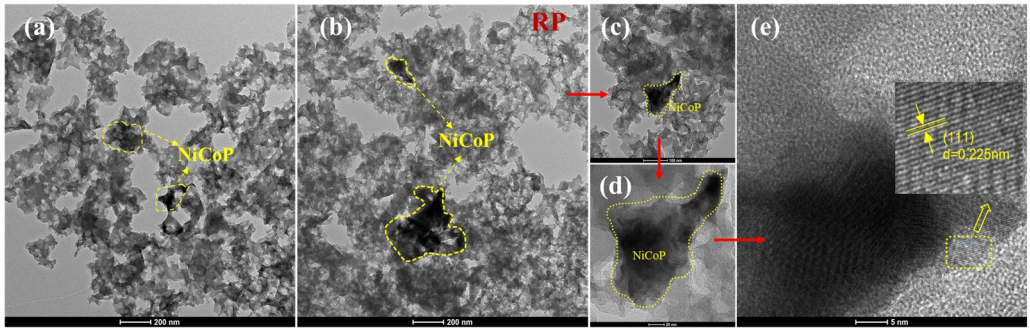

Figure 2. (a-d) TEM and (e) HRTEM images of 6% NiCoP/RP.

DOI: 10.14102/j.cnki.0254-5861.2021-0055

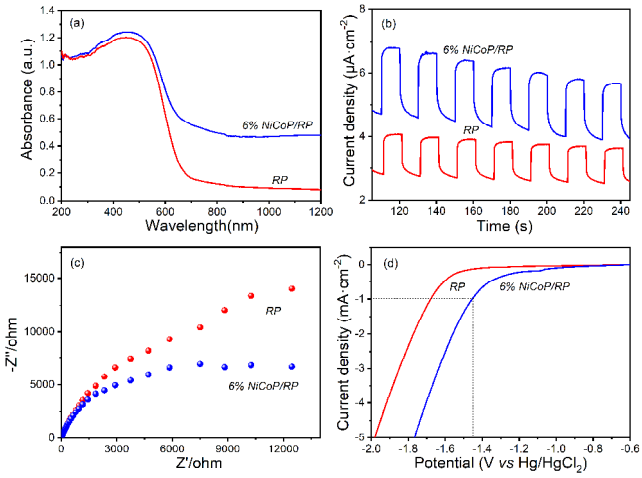

Figure 4. (a) UV-Vis absorption spectra, (b) I-t curves, (c) EIS and (d) linear sweep voltammetry curves of the samples.

of Co^{2+}, the signal of 782.2 eV may be related to Co^{3+}, the peak at 793.4 eV belongs to the P-Co bond in the complex, and the signals at 786.5 and 803.4 eV are the two satellite peaks of Co 2*p*.[52] The peaks at 853.1 eV ($2p_{1/2}$) and 870.3 eV ($2p_{3/2}$) in Figure 3c correspond to Ni^{2+}, and those at 856.5 and 874.2 eV belong to $Ni^{\delta+}$ ($0<\delta<2$) in NiCoP. The signals at 861.1 and 880.2 eV are the satellite peaks of Ni 2*p*.[53,54] From the P 2*p* high resolution XPS spectra in Figure 3d, the signals at 129.6 and 133.3 eV result from $P^{\delta-}$ and PO_4^{3-}, respectively. The peak at 130.4 eV of pure RP in Figure 3d is attributed to P 2*p*, and that at 134.8 eV belongs to P-O bond resulting from the oxidization of RP in air, which is the characteristic peak of P^{5+}.[55,56] Compared with pure RP, the binding energy of P element shifts towards lower direction in the complex, indicating the formation of M-P bond (M = Co or Ni), thus making the P atom partially negatively charged.[55,57]

Photoelectric Performance. The optical absorption of the samples was revealed by UV-Vis absorption spectra in Figure 4a. The absorption edge of pure RP is located at 700 nm.[58] The light harvest capacity of the composite is obviously enhanced after loading NiCoP, which can be attributed to the black color of NiCoP sample.[59] In addition, the PL intensity of 6% NiCoP/RP is obviously lower than that of RP in Figure S5, indicating NiCoP can inhibit electron and hole recombination.[48,60] The transient photocurrent response of the samples was measured by electrochemical workstation. As shown in Figure 4b, both samples show quick photocurrent response when the light source is on and off, and the photocurrent density of 6% NiCoP/RP is higher than that of RP, indicating that the introduction of NiCoP improves the separation efficiency of electrons and holes.[61] Figure 4c shows the electrochemical impedance spectroscopy (EIS) of the samples. 6% NiCoP/RP has a smaller radius of EIS curve, suggesting NiCoP can reduce the transfer resistance of charge carriers, which is conducive to the migration of charge carriers.[62,63] The polarization curve measured in 0.5 mol·L^{-1} Na_2SO_4 solution in Figure 4d indicates that NiCoP can also reduce the H_2 production overpotential of RP effectively. When the current density is -1 mA·cm^{-2}, the H_2 production overpotential (-1.45 V vs. SCE) of 6%

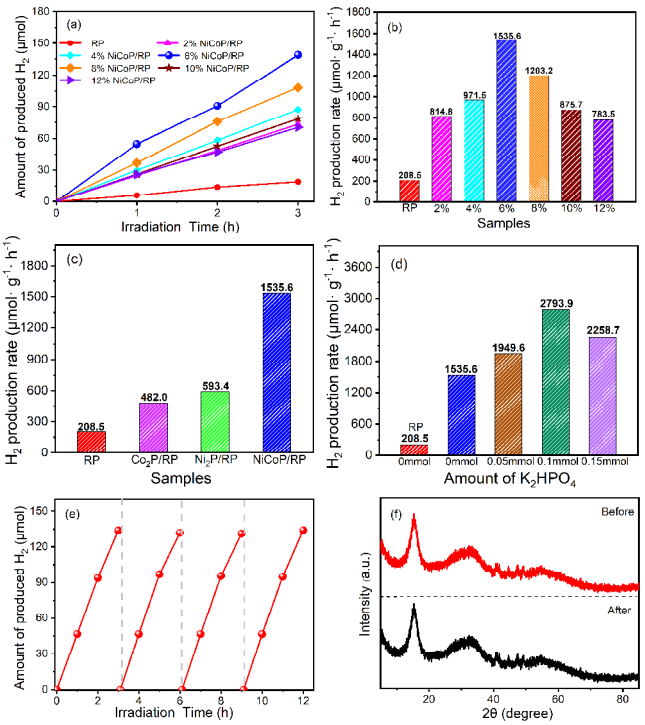

Figure 5. (a) Photocatalytic H_2 production performance of the samples, (b) the average H_2 production rate for 3 h, (c) H_2 production rate of different samples, (d) the effect of K_2HPO_4 amount on the average H_2 production rate of 6%NiCoP/RP, (e) the cycle H_2 production curves and (f) XRD patterns of before and after used of samples.

NiCoP/RP is lower than that of RP (-1.68 V vs. SCE), implying NiCoP/RP has faster reduction/oxidation surface reaction kinetics.[43,64]

H_2 Production Activity. Figure 5a-b show the H_2 production curves of the samples and corresponding H_2 evolution rate. With the increase of NiCoP content, the activity of the composite increases significantly. The 6% NiCoP/RP heterojunction has the best activity with an average H_2 production rate of 1535.6 μmol·g^{-1}·h^{-1}, which is 7.4 times higher than that of pure RP (208.5 μmol·g^{-1}·h^{-1}). However, the activity of the composite decreases when overloading NiCoP, which may result from the "shielding effect" caused by excessive NiCoP, leading to a lower light absorption of RP.[47] Figure 5c shows the activity of different composites modified by Ni_2P, Co_2P and NiCoP, respectively. The H_2 production rates of 6% Ni_2P/RP and 6% Co_2P/RP are respectively 593.4 and 482.0 μmol·g^{-1}·h^{-1}, although they are higher than that of pure RP, but lower than that of 6% NiCoP/RP. This is largely due to the synergistic effect of nickel and cobalt, making NiCoP have stronger conductivity than Co_2P and Ni_2P.[65] In addition, the Gibbs adsorption energy (ΔG_{H^*}) of NiCoP for the active species (H*) in the reaction solution is smaller than that of single metal, which makes NiCoP more conducive to the formation of H-H bond and the desorption of H_2 on the surface. Alshareef et al. have proved the ΔG_{H^*} on the NiCoP (0001) surface is low based on DFT results. The *d*-states of NiCoP are found closer to the Fermi level which

Chin. J. Struct. Chem. **2022**, 41, 2206062-2206068
DOI: 10.14102/j.cnki.0254-5861.2021-0055

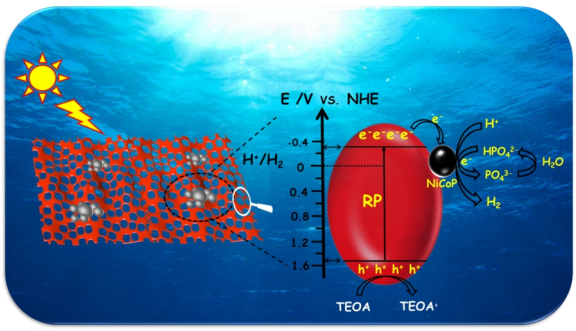

Figure 6. Schematic illustration of photocatalytic H_2 production mechanism over 6% NiCoP/RP promoted by HPO_4^{2-}.

points to a lower intermedia adsorption energy,[66] and further enhances the catalytic activity of the complex.[54,59,67] Some works about NiCoP cocatalyst in the photocatalysis have been summarized in Table S1. Obviously, NiCoP can greatly improve the activity of different photocatalysts.

In nature, photosynthesis is accomplished through the cooperation of a series of pigment protein complexes embedded in the cell membrane, during which phospholipid molecules take a leading role in the electron transfer and synthesis of adenosine triphosphate.[68] Inspired by the phosphate-involving natural photosynthesis, in order to improve the H_2 production rate of the catalyst, the K_2HPO_4 was applied to simulate the phosphate molecules, as shown in Figure 5d. When the trace amount of K_2HPO_4 is added to the reaction solution, the activity of 6% NiCoP/RP is significantly improved. After adding 0.1 mmol K_2HPO_4 in 100 mL reaction solution, the average H_2 production rate reaches 2793.9 $\mu mol \cdot g^{-1} \cdot h^{-1}$, which is 13.4 and 1.8 times higher than those of pure RP and 6% NiCoP/RP without K_2HPO_4, respectively. However, excessive K_2HPO_4 might affect the pH of the solution or the surface active state of the photocatalyst, resulting in a poor activity. In fact, Ye et al. have discovered that the existence of HPO_4^{2-} can improve the activity of g-C_3N_4 systems. However, there are few studies on the photocatalytic H_2 production under this "phosphorylation" environment. It is found that HPO_4^{2-} can shorten the proton reduction cycle, and also reduce the oxidation potential of TEOA, thus accelerating the carrier utilization efficiency in the reaction.[69]

The stability of the samples was tested *via* photocatalytic H_2 production cycling experiment (See the supporting materials). As shown in Figure 5e, the activity of 6% NiCoP/RP changes slightly during the 4 cycles of 12 h. Besides, there is no change about the crystal structure of the sample after using (Figure 5f), indicating NiCoP/RP heterojunction has good structural stability during H_2 production.

Mechanism Analysis. In order to investigate the H_2 evolution mechanism of NiCoP/RP composite sample, the band structure of RP nanosheets was calculated by Tauc plots and XPS in Figure S6. According to the above results, the process of photocatalytic H_2 production over NiCoP/RP heterojunction is presented in Figure 6. Under illumination, the electrons in the valence band (VB) of RP nanosheets transfer to the conduction band (CB).[47] Subsequently, electrons in the CB of RP will quickly migrate to NiCoP and participate in the proton reduction reaction, while the holes in the VB will react with the sacrificial agent efficiently. In addition, HPO_4^{2-} in reaction solution can provide a large amount of H^+ to participate in the reaction at the active site to produce H_2 and PO_4^{3-}, and the generated PO_4^{3-} will combine with H^+ in water to form HPO_4^{2-} and participate in the H_2 production again. Therefore, HPO_4^{2-} can act as a mediator to promote H_2 production, resulting in a new proton reduction pathway, which can further improve the photocatalytic H_2 production rate of the NiCoP/RP heterojunction.

n CONCLUSION

NiCoP/RP heterostructure was constructed by a combination of solvothermal method and physical grinding processes. Bimetallic NiCoP/RP exhibits higher catalytic H_2 production activity than single metal phosphides Ni_2P/RP and Co_2P/RP during photocatalytic H_2 evolution. NiCoP can not only facilitate carrier migration, but also reduce the interface impedance and H_2 production overpotential, resulting in better H_2 production rate of 1535.6 $\mu mol \cdot g^{-1} \cdot h^{-1}$ over 6% NiCoP/RP, which is 7.4, 3.2 and 2.6 times higher than that of RP (208.5 $\mu mol \cdot g^{-1} \cdot h^{-1}$), 6% Co_2P/RP (482.0 $\mu mol \cdot g^{-1} \cdot h^{-1}$) and 6% Ni_2P/RP (593.4 $\mu mol \cdot g^{-1} \cdot h^{-1}$), respectively. In addition, the H_2 production rate of 6% NiCoP/RP is further increased to 2793.9 $\mu mol \cdot g^{-1} \cdot h^{-1}$ after adding K_2HPO_4 for the "phosphorylation" environment. It is 1.8 times higher than that of 6% NiCoP/RP without K_2HPO_4. This work may provide a new idea for improving the photocatalytic H_2 production using bimetallic phosphide cocatalysts and suitable electrolyte.

n EXPERIMENTAL SECTION

The detailed information about chemicals was added to the supporting materials.

Synthesis of Nanosized RP. Nanosized RP was prepared by a hydrothermal method using commercial micron RP as the P sources.[70] The commercial micron RP was ground with water and filtered through a 120 mesh sieve, and then dried for 12 h. Subsequently, 3.0 g obtained RP was dispersed in 60 mL of water, sealed in a 100 mL Teflon-lined autoclave, then heated to 200 °C and kept for 12 h. Finally, the product was centrifuged, washed for three times with water after cooling down, and dried in the oven at 60 ℃ to obtain nanosized RP.

Synthesis of Co_2P and Ni_2P Nanoparticles. Co_2P and Ni_2P NPs were prepared by a solvothermal method[47]. Firstly, a certain amount of $CoCl_2 \cdot 6H_2O$ was dissolved in the mixed solvent of 25 mL of water and 25 mL of ethanol. 0.4 g nano RP, 0.10 g cetyl trimethyl ammonium bromide (CTAB) and 0.10 g sodium dodecyl benzene sulfonate (SDBS) were added into the above solution. After stirring for 30 min, they were transferred to a 100 mL Teflon-lined autoclave, sealed and heated at 200 ℃ for 10 h. The products were centrifuged, washed and dried to obtain Co_2P NPs. The Ni_2P was obtained by similar procedures by using $CoCl_2 \cdot 6H_2O$ instead of $NiCl_2 \cdot 6H_2O$, and the reaction temperature was maintained at 180 ℃ for 12 h.

Synthesis of NiCoP Nanoparticles. NiCoP NPs were prepared by a solvothermal method, too. First, *x* mmol $NiCl_2 \cdot 6H_2O$ and (2-*x*) mmol $CoCl_2 \cdot 6H_2O$ (*x* = 0.5, 1, 1.25 and 1.5 mmol, respectively)

DOI: 10.14102/j.cnki.0254-5861.2021-0055

were dissolved in the bi-component solvent of 15 mL of ethylene glycol and 45 mL of ethanol. Subsequently, 0.78 g RP and 0.10 g polyvinylpyrrolidone (PVP) were added into the above solution. After stirring for 30 min, it was transferred into a 100 mL Teflon-lined autoclave, sealed and heated to 200 °C for 20 h. After cooling naturally, bimetallic NiCoP was obtained after centrifugation, washing and drying the black precipitate. They are labeled as $Ni_{0.5}Co_{1.5}P$, $Ni_{1.0}Co_{1.0}P$ (NiCoP), $Ni_{1.25}Co_{0.75}P$ and $Ni_{1.5}Co_{0.5}P$, corresponding to x = 0.5, 1, 1.25 and 1.5 mmol, respectively.

Preparation of NiCoP/RP Composites. The NiCoP/RP composites were prepared by a physical grinding process. As shown in Figure S1, 200.0 mg of nanosized RP and NiCoP NPs (4.0, 8.0, 12.0, 16.0, 20.0, or 24.0 mg) were poured into an agate mortar containing 60.0 mL of water. After 30 min physical grinding, the mixture was dried at 60 °C for 12 h, with the product labeled as x% NiCoP/RP (x is the mass fraction of NiCoP in the composites, and x is 2, 4, 6, 8, 10 and 12, respectively). Co_2P/RP and Ni_2P/RP are obtained using Co_2P or Ni_2P NPs to replace NiCoP during the above processes.

Characterization. The photoelectric and photocatalytic experiments and other characterizations are given in the supporting materials.

n ACKNOWLEDGEMENTS

This work was supported by the National Natural Science Foundation of China (Nos. 22078261, 21676213, and 11974276), and the Natural Science Basic Research Program of Shaanxi (No. 2020JM-422).

n AUTHOR INFORMATION

Corresponding authors. Emails: liuenzhou@nwu.edu.cn (Enzhou Liu) and zhaobr@nwu.edu.cn (Binran Zhao)

n COMPETING INTERESTS

The authors declare no competing interests.

n ADDITIONAL INFORMATION

Supplementary information is available for this paper at http://manu30.magtech.com.cn/jghx/EN/10.14102/j.cnki.0254-5861.2021-0055

For submission: https://mc03.manuscriptcentral.com/cjsc

n REFERENCES

(1) Xu, F.; Meng, K.; Cheng, B.; Wang, S.; Xu, J.; Yu, J. Unique S-scheme heterojunctions in self-assembled TiO_2/$CsPbBr_3$ hybrids for CO_2 photoreduction. *Nat. Commun.* **2020**, 11, 4613.

(2) Liang, Z.; Shen, R.; Ng, Y. H.; Zhang, P.; Xiang, Q.; Li, X. A review on 2D MoS_2 cocatalysts in photocatalytic H_2 production. *J. Mater. Sci. Technol.* **2020**, 56, 89-121.

(3) Jiang, Z.; Chen, Q.; Zheng, Q.; Shen, R.; Zhang, P.; Li, X. Constructing 1D/2D Schottky-based heterojunctions between $Mn_{0.2}Cd_{0.8}S$ nanorods and Ti_3C_2 nanosheets for boosted photocatalytic H_2 evolution. *Acta Phys. Chim. Sin.* **2021**, 37, 2010059.

(4) Fujishima, A.; Honda, K. Electrochemical photolysis of water at a semiconductor electrode. *Nature* **1972**, 238, 37-38.

(5) Xu, J.; Huang, J.; Wang, Z.; Zhu, Y. Enhanced visible-light photocatalytic degradation and disinfection performance of oxidized nanoporous g-C_3N_4 *via* decoration with graphene oxide quantum dots. *Chin. J. Catal.* **2020**, 41, 474-484.

(6) Xia, Y.; Yu, J. Reaction: rational design of highly active photocatalysts for CO_2 conversion. *Chem.* **2020**, 6, 1035-1042.

(7) Ren, D.; Shen, R.; Jiang, Z.; Lu, X.; Li, X. Highly efficient visible-light photocatalytic H_2 evolution over 2D-2D CdS/Cu_7S_4 layered heterojunctions. *Chin. J. Catal.* **2020**, 41, 31-40.

(8) Yu, J.; Li, X.; Ong, W. J.; Zhang, L. Design and fabrication of advanced photocatalysts. *Acta Phys. Chim. Sin.* **2021**, 37, 2012043.

(9) Wang, Z.; Hong, J.; Ng, S. F.; Liu, W.; Huang, J.; Chen, P.; Ong, W. J. recent progress of perovskite oxide in emerging photocatalysis landscape: water splitting, CO_2 reduction, and N_2 fixation. *Acta. Phys. Chim. Sin.* **2021**, 37, 2011033.

(10) Xia, P.; Cao, S.; Zhu, B.; Liu, M.; Shi, M.; Yu, J.; Zhang Y. Designing a 0D/2D S-scheme heterojunction over polymeric carbon nitride for visible-light photocatalytic inactivation of bacteria. *Angew. Chem. Int. Ed.* **2020**, 59, 5218-5225.

(11) Lin, W. C.; Jayakumar, J.; Chang, C. L.; Ting, L. Y.; Elsayed, M. H.; Abdellah, M.; Zheng, K.; Elewa, A. M.; Lin, Y. T.; Liu, J. J.; Wang, W. S.; Lu, C. Y.; Chou, H. H. Effect of energy bandgap and sacrificial agents of cyclopentadithiophene-based polymers for enhanced photocatalytic hydrogen evolution. *Appl. Catal. B Environ.* **2021**, 298, 120577.

(12) Wang, R.; Shi, M.; Xu, F.; Qiu, Y.; Zhang, P.; Shen, K.; Zhao, Q.; Yu, J.; Zhang, Y. Graphdiyne-modified TiO_2 nanofibers with osteoinductive and enhanced photocatalytic antibacterial activities to prevent implant infection. *Nat. Commun.* **2020**, 11, 4465.

(13) Chen, B. B.; Liu, S. Q.; Weng, S. X. Template-free polyoxometalate-assisted synthesis of Au/ZnO hollow sphere hererostructures for photocatalytic water purification. *Chin. J. Struct. Chem.* **2018**, 37, 924-936.

(14) Wang, Y. Q.; Liu, Y.; Zhang, M. X.; Min, F. F. Electronic, magnetic and photocatalytic properties in (Fe, Ni)-codoped $SrTiO_3$ with and without oxygen vacancies: a first-principles study. *Chin. J. Struct. Chem.* **2018**, 37, 1025-1036.

(15) Lei, Z.; Ma, X.; Hu, X.; Fan, J.; Liu, E. Enhancement of photocatalytic h_2-evolution kinetics through the dual cocatalyst activity of Ni_2P-NiS-decorated g-C_3N_4 heterojunctions. *Acta Phys. Chim. Sin.* **2022**, 38, 2110049.

(16) Shen, R.; Ren, D.; Ding, Y.; Guan, Y.; Ng, Y. H.; Zhang P.; Li, X. Nanostructured CdS for efficient photocatalytic H_2 evolution: a review. *Sci. China Mater.* **2020**, 63, 2153-2188.

(17) Feng, K.; Xue, W.; Hu, X.; Fan, J.; Liu, E. Z-scheme CdSe/ZnSe heterojunction for efficient photocatalytic hydrogen evolution. *Colloids Surf. A* **2021**, 622, 126633.

(18) Liu, D.; Chen, S.; Li, R.; Peng, T. Review of Z-scheme heterojunctions for photocatalytic energy conversion. *Acta Phys. Chim. Sin.* **2021**, 37, 2010017.

(19) Wang, F.; Ng, W. K. H.; Yu, J. C.; Zhu, H.; Li, C.; Zhang, L.; Liu, Z.; Li, Q. Red phosphorus: an elemental photocatalyst for hydrogen formation from water. *Appl. Catal. B Environ.* **2012**, 111-112, 409-414.

(20) Zhu, Y.; Ren, J.; Zhang, X.; Yang, D. Elemental red phosphorus-based materials for photocatalytic water purification and hydrogen production. *Nanoscale* **2020**, 12, 13297.

(21) Hu, Z.; Yuan, L.; Liu, Z.; Shen, Z.; Yu, J. C. An elemental phosphorus photocatalyst with a record high hydrogen evolution efficiency. *Angew. Chem. Int. Ed.* **2016**, 55, 1-7.

DOI: 10.14102/j.cnki.0254-5861.2021-0055

(22) Jia, J.; Bai, X.; Zhang, Q.; Hu, X.; Liu, E.; Fan, J. Porous honeycomb-like $NiSe_2$/red phosphorus heteroarchitectures for photocatalytic hydrogen production. *Nanoscale* **2020**, 12, 5636.
(23) Kuang, P.; Sayed, M.; Fan, J.; Cheng, B.; Yu, J. 3D Graphene-based H_2-production photocatalyst and electrocatalyst. *Adv. Energy Mater.* **2020**, 10, 1903802.
(24) Ren, Z.; Li, D.; Xue, Q.; Li, J.; Sun, Y.; Zhang, R.; Zhai, Y.; Liu, Y. Facile fabrication nano-sized red phosphorus with enhanced photocatalytic activity by hydrothermal and ultrasonic method. *Catal. Today* **2020**, 340, 115-120.
(25) Xu, Q.; Zhang, L.; Cheng, B.; Fan, J.; Yu, J. S-scheme heterojunction photocatalyst. *Chem.* **2020**, 6, 1543-1559.
(26) Li, Y.; Zhang, M.; Zhou, L.; Yang, S.; Wu, Z.; Ma, Y. Recent advances in surface-modified g-C_3N_4-based photocatalysts for H_2 production and CO_2 reduction. *Acta Phys. Chim. Sin.* **2021**, 37, 2009030.
(27) Tang, S.; Xia, Y.; Fan, J.; Cheng, B.; Yu, J.; Ho, W. Enhanced photocatalytic H_2 production performance of CdS hollow spheres using C and Pt as bi-cocatalysts. *Chin. J. Catal.* **2021**, 42, 743-752.
(28) Wang, P.; Cao, Y.; Xu, S.; Yu, H. Boosting the H_2-evolution performance of TiO_2/Au photocatalyst by the facile addition of thiourea molecules. *Appl. Surf. Sci.* **2020**, 532, 147420.
(29) Liu, M. M.; Ying, S. M.; Chen, B. G.; Guo, H. X.; Huang, X. G. Ag@g-C_3N_4 nanocomposite: an efficient catalyst inducing the reduction of 4-nitrophenol. *Chin. J. Struct. Chem.* **2021**, 40, 1372-1378.
(30) Tong, R.; Ng, K. W.; Wang, X.; Wang, S.; Wang, X.; Pan, H. Two-dimensional materials as novel co-catalysts for efficient solar-driven hydrogen production. *J. Mater. Chem. A* **2020**, 8, 23202.
(31) Shen, R.; He, K.; Zhang, A.; Li, N.; Ng, Y. H.; Zhang, P.; Hu, J.; Li, X. In-situ construction of metallic Ni_3C@Ni core-shell cocatalysts over g-C_3N_4 nanosheets for shell-thickness-dependent photocatalytic H_2 production. *Appl. Catal. B-Environ.* **2021**, 291, 120104.
(32) Wu, Y.; Wang, H.; Ji, S.; Pollet, B. G.; Wang, X.; Wang, R. Engineered porous Ni_2P-nanoparticle/Ni_2P-nanosheet arrays *via* the Kirkendall effect and Ostwald ripening towards efficient overall water splitting. *Nano Res.* **2020**, 13, 2098-2105.
(33) Sun, H.; Xue, W.; Fan, J.; Liu, E.; Yu, Q. Preparation of $Ni_{12}P_5$-decorated $Cd_{0.5}Zn_{0.5}S$ for efficient photocatalytic H_2 evolution. *J. Alloys Compd.* **2021**, 854, 156951.
(34) Ali, A.; Liu, Y.; Mo, R.; Chen, P.; Shen, P. K. Facile one-step in-situ encapsulation of non-noble metal Co_2P nanoparticles embedded into B, N, P tri-doped carbon nanotubes for efficient hydrogen evolution reaction. *Int. J. Hydrogen Energy* **2020**, 45, 24312-24321.
(35) Fu, Z.; Ma, X.; Xia, B.; Hu, X.; Fan, J.; Liu, E. Efficient photocatalytic H_2 evolution over Cu and Cu_3P co-modified TiO_2 nanosheet. *Int. J. Hydrogen Energy* **2021**, 46, 19373-19384.
(36) Pan, J.; Ou, W.; Li, S.; Chen, Y.; Li, H.; Liu, Y.; Wang, J.; Song, C.; Zheng, Y.; Li, C. Photocatalytic hydrogen production enhancement of Z-Scheme CdS quantum dots/Ni_2P/Black Ti^{3+}-TiO_2 nanotubes with dual-functional Ni_2P nanosheets. *Int. J. Hydrogen Energy* **2020**, 45, 33478-33490.
(37) Ray, A.; Sultana, S.; Paramanik, L.; Parida, K. M. Recent advances in phase, size, and morphology-oriented nanostructured nickel phosphide for overall water splitting. *J. Mater. Chem. A* **2020**, 8, 19196-19245.
(38) Ren, D.; Liang, Z.; Ng, Y. H.; Zhang, P.; Xiang, Q.; Li, X. Strongly coupled 2D-2D nanojunctions between P-doped Ni_2S (Ni_2SP) cocatalysts and CdS nanosheets for efficient photocatalytic H_2 evolution. *Chem. Eng. J.* **2020**, 390, 124496.
(39) Yan, X.; Wang, G.; Zhang, Y.; Guo, Q.; Jin, Z. 3D layered nano-flower MoS_x anchored with CoP nanoparticles form double proton adsorption site for enhanced photocatalytic hydrogen evolution under visible light driven. *Int. J. Hydrogen Energy* **2020**, 45, 2578-2592.
(40) Cai, J.; Song, Y.; Zang, Y.; Niu, S.; Wu, Y.; Xie, Y.; Zheng, X.; Liu, Y.; Lin, Y.; Liu, X.; Wang, G.; Qian, Y. N-induced lattice contraction generally boosts the hydrogen evolution catalysis of P-rich metal phosphides. *Sci. Adv.* **2020**, 6, 8113.
(41) Zhang, Y.; Wang, J.; Shi, X.; Zhang, P.; Ning, W.; Li, W.; Wei, C.; Miao, S. Prolonged-photoresponse-lifetime Ni_2P nanocrystalline with highly exposed (001) for efficient photoelectrocatalytic hydrogen evolution. *Inorg. Chem.* **2021**, 60, 16439-16446.
(42) Zhang, J.; Zhou, H.; Liu, Y.; Zhang, J.; Cui, Y.; Li, J.; Lian, J.; Wang, G.; Jiang, Q. Interface engineering of CoP_3/Ni_2P for boosting the wide pH range water-splitting activity. *ACS Appl. Mater. Inter.* **2021**, 13, 52598-52609.
(43) Sun, Y.; Ren, Z.; Liu, Y.; Fu, R. Facile synthesis of ultrathin red phosphorus nanosheets with excellent photocatalytic performances. *Mater. Lett.* **2019**, 236, 542-546.
(44) Li, C.; Fu, M.; Wang, Y.; Liu, E.; Fan, J.; Hu, X. In situ synthesis of Co_2P-decorated red phosphorus nanosheets for efficient photocatalytic H_2 evolution. *Catal. Sci. Technol.* **2020**, 10, 2221-2230.
(45) Bi, L.; Gao, X.; Zhang, L.; Wang, D.; Zou, X.; Xie, T. Enhanced photocatalytic hydrogen evolution of NiCoP/g-C_3N_4 with improved separation efficiency and charge transfer efficiency. *ChemSusChem.* **2018**, 11, 276-284.
(46) Liang, L. L.; Song, G.; Liu, Z.; Chen, J. P.; Xie, L. J.; Jia, H.; Kong, Q. Q.; Sun, G. H.; Chen, C. M. Constructing $Ni_{12}P_5$/Ni_2P heterostructures to boost interfacial polarization for enhanced microwave absorption performance. *ACS Appl. Mater. Inter.* **2020**, 12, 52208-52220.
(47) Tang, C.; Zhang, R.; Lu, W.; Wang, Z.; Liu, D.; Hao, S.; Du, G.; Asiri, A. M.; Sun, X. Energy-saving electrolytic hydrogen generation: Ni_2P nanoarray as a high-performance non-noble-metal electrocatalyst. *Angew. Chem. Int. Ed.* **2017**, 56, 842-846.
(48) Sun, X.; Liu, H.; Xu, G.; Bai, J.; Li, C. Embedding Co_2P nanoparticles into N&P co-doped carbon fibers for hydrogen evolution reaction and supercapacitor. *Int. J. Hydrogen Energy* **2021**, 46, 1560-1568.
(49) Cao, H.; Wang, T.; Minja, A. C.; Jiang, D.; Du, P. NiCoP nanoparticles anchored on CdS nanorods for enhanced hydrogen production by visible light-driven formic acid dehydrogenation. *Int. J. Hydrogen Energy* **2021**, 46, 32435-32444.
(50) Zhang, Y.; Mollon, G.; Descartes, S. Significance of third body rheology in friction at a dry sliding interface observed by a multibody meshfree model: influence of cohesion between particles. *Tribol. Int.* **2020**, 145, 106188.
(51) Bai, J.; Zhou, P.; Xu, P.; Deng, Y.; Zhou, Q. Synergy of dopants and porous structures in graphitic carbon nitride for efficient photocatalytic H_2 evolution. *Ceram. Int.* **2021**, 47, 4043-4048.
(52) Chen, Y.; Xu, Y.; Lin, D.; Luo, Y.; Xue, H.; Chen, Q. Insight into superior visible light photocatalytic activity for degradation of dye over corner-truncated cubic Ag_2O decorated TiO_2 hollow nanofibers. *Chin. J. Struct. Chem.* **2020**, 39, 588-597.
(53) Qin, Z.; Chen, Y.; Huang, Z.; Su, J.; Guo, L. A bifunctional NiCoP-based core/shell cocatalyst to promote separate photocatalytic hydrogen and oxygen generation over graphitic carbon nitride. *J. Mater. Chem. A.* **2017**, 5, 19025.

DOI: 10.14102/j.cnki.0254-5861.2021-0055

(54) Du, C.; Yang, L.; Yang, F.; Cheng, G.; Luo, W. Nest-like NiCoP for highly efficient overall water splitting. *ACS Catal.* **2017**, 7, 4131-4137.

(55) Dang, T.; Zhang, G.; Li, Q.; Cao, Z.; Zhang, G.; Duan, H. Ultrathin hetero-nanosheets assembled hollow Ni-Co-P/C for hybrid supercapacitors with enhanced rate capability and cyclic stability. *J. Colloid Interface Sci.* **2020**, 577, 368-378.

(56) Yu, C.; Xu, F.; Luo, L.; Abbo, H. S.; Titinchi, S. J. J.; Shen, P. K.; Tsiakaras, P.; Yin, S. Bimetallic Ni-Co phosphide nanosheets self-supported on nickel foam as high-performance electrocatalyst for hydrogen evolution reaction. *Electrochim. Acta* **2019**, 317, 191-198.

(57) Ray, C.; Lee, S. C.; Jin, B.; Kundu, A.; Park, J. H.; Jun, S. C. Stacked porous iron-doped nickel cobalt phosphide nanoparticle: an efficient and stable water splitting electrocatalyst. *ACS Sustain. Chen. Eng*. **2018**, 6, 6146-6156.

(58) Wang, Y.; Shen, G.; Zhang, Y.; Pan, L.; Zhang, X.; Zou, J. J. Visible-light-induced unbalanced charge on NiCoP/TiO_2 sensitized system for rapid H_2 generation from hydrolysis of ammonia borane. *Appl. Catal. B Environ.* **2020**, 260, 118183.

(59) Qi, L.; Dong, K.; Zeng, T.; Liu, J.; Fan, J.; Hu, X.; Jia, W.; Liu, E. Three-dimensional red phosphorus: a promising photocatalyst with excellent adsorption and reduction performance. *Catal. Today* **2018**, 314, 42-51.

(60) Zeng, L.; Sun, K.; Wang, X.; Liu, Y.; Pan, Y.; Liu, Z.; Cao, D.; Song, Y.; Liu, S.; Liu, C. Three-dimensional-networked Ni_2P/Ni_3S_2 hetero-nanoflake arrays for highly enhanced electrochemical overall-water-splitting activity. *Nano Energy* **2018**, 51, 26-36.

(61) Zhang, J.; Liao, H.; Sun, S. Construction of 1D/1D WO_3 nanorod/TiO_2 nanobelt hybrid heterostructure for photocatalytic application. *Chin. J. Struct. Chem.* **2020**, 39, 1019-1028.

(62) Zhai, C.; Zhu, M.; Ren, F.; Yao, Z.; Du, Y.; Yang, P. Enhanced photoelectrocatalytic performance of titanium dioxide/carbon cloth based photoelectrodes by graphene modification under visible-light irradiation. *J. Hazard. Mater.* **2013**, 263, 291-298.

(63) Xue, W.; Bai, X.; Tian, J.; Ma, X.; Hu, X.; Fan, J.; Liu, E. Enhanced photocatalytic H_2 evolution on ultrathin $Cd_{0.5}Zn_{0.5}S$ nanosheets without a hole scavenger: combined analysis of surface reaction kinetics and energy-level alignment. *Chem. Eng. J.* **2022**, 428, 132608.

(64) Zhang, K.; Fujitsuka, M.; Du, Y.; Majima, T. 2D/2D heterostructured CdS/WS_2 with efficient charge separation improving H_2 evolution under visible light irradiation. *ACS Appl. Mater. Interfaces* **2018**, 10, 20458-20466.

(65) Liu, H.; Su, P.; Jin, Z.; Ma, Q. Enhanced hydrogen evolution over sea-urchin-structure NiCoP decorated ZnCdS photocatalyst. *Catal. Lett.* **2020**, 150, 2937-2950.

(66) Zhang, X.; Wu, A.; Wang, X.; Tian, C.; An, R.; Fu, H. Porous NiCoP nanosheets as efficient and stable positive electrodes for advanced asymmetric supercapacitors. *J. Mater. Chem. A* **2018**, 6, 17905.

(67) Liang, H.; Gandi, A. N.; Anjum, D. H.; Wang, X.; Schwingenschlögl, U.; Alshareef, H. N. Plasma-assisted synthesis of NiCoP for efficient overall water splitting. *Nano Lett*. **2016**, 16, 7718-7725.

(68) Lai, C.; Liu, X.; Wang, Y.; Cao, C.; Yin, Y.; Yang, H.; Qi, X.; Zhong, S.; Hou, X.; Liang, T. Modulating ternary Mo-Ni-P by electronic reconfiguration and morphology engineering for boosting all-pH electrocatalytic overall water splitting. *Electrochim. Acta* **2020**, 330, 135294.

(69) Shi, L.; Chang, K.; Zhang, H.; Hai, X.; Yang, L.; Wang, T.; Ye, J. Drastic enhancement of photocatalytic activities over phosphoric acid protonated porous g-C_3N_4 nanosheets under visible light. *Small* **2016**, 12, 4431-4439.

(70) Liu, G.; Wang, T.; Zhang, H.; Meng, X.; Hao, D.; Chang, K.; Li, P.; Kako, T.; Ye, J. Nature-inspired environmental "phosphorylation" boosts photocatalytic H_2 production over carbon nitride nanosheets under visible-light irradiation. *Angew. Chem. Int. Ed.* **2015**, 54, 13561-13565.

Received: December 16, 2021
Accepted: January 29, 2022
Published: June 20, 2022

DOI: 10.14102/j.cnki.0254-5861.2021-0055